Journal of Wind Engineering & Industrial Aerodynamics 227 (2022) 105073

Contents lists available at ScienceDirect

Journal of Wind Engineering & Industrial Aerodynamics

journal homepage: www.elsevier.com/locate/jweia

Flight characteristics of rod-shaped windborne debris objects in atmospheric boundary layer winds

Dikshant Saini, Behrouz Shafei *

Department of Civil, Construction, and Environmental Engineering, Iowa State University, Ames, IA, 50011, USA

ARTICLE INFO

Keywords:
Rod-shaped debris
Atmospheric boundary layer wind
Simulation framework
Impact energy
Pitch and yaw angles

ABSTRACT

The presented study explored the flight characteristics of rod-shaped debris objects in neutrally-stratified atmospheric boundary layer (ABL) winds. Despite the fact that rod-shaped debris objects, such as lumbers, are a common type of debris observed during extreme wind events, their three-dimensional motions had not been fully characterized and the understanding of their flight trajectories was limited to the outcome of only a few wind tunnel tests. To address the outlined research gaps, this study established a coupled simulation framework, which utilized both computational fluid dynamics (CFD) and rigid body dynamics (RBD). After validating this framework using the experimental test data, the flight trajectories of a set of rod-shaped debris objects were first evaluated in uniform winds. With placing the rod's longitudinal axis in both along-wind and cross-wind directions, the debris flight motions were characterized for various initial pitch angles. After appropriate verifications, the simulations were extended to investigate the flight of rod-shaped objects in ABL winds. The main debris flight properties, including displacement and velocity profiles, were systematically extracted over time, taking into consideration various influential factors. With the wealth of debris flight data generated through the conducted CFD-RBD simulations, predictive models were developed for assessing the kinetic energy associated with the flight of rod-shaped debris objects.

1. Introduction

In high-wind regions, building envelopes are subjected to various extreme events, such as hurricanes and tornados. Past events show that wind-induced damage to building envelope components can result in significant direct and indirect losses every year. Among the main contributing mechanisms, the impact due to windborne debris is known to be detrimental, as building envelope components are directly targeted. In Lubbock Storm (1970), windborne debris was reported as the leading cause of damage, especially to windows. Similar observations were made following Hurricane Celia (1970) and Tropical Cyclone Tracy (1974), as reported in Minor (1994). From the reconnaissance study conducted after Hurricane Alicia (1983), windborne debris originated from building roofs caused most of damage to architectural glazing systems. Similar situations concerning the consequences of windborne debris were observed after Hurricane Charley (2004) and Hurricane Katrina (2005), which caused extensive damage to buildings and other structures (FEMA, 2011 and 2015). In the event of debris impact, the moving debris can penetrate into the building envelope. This can create excessive internal pressure, and thus, increase the net load that the roof and surrounding walls witness. As a result, failed roof and wall components can become a new source of debris. As more debris objects are separated from buildings and other structures, more damage to their surroundings is anticipated. Therefore, it is critical to have a thorough understanding of the flight characteristics of various debris objects during extreme wind events.

For the evaluation of the windborne debris impact resistance of building envelope components, the current design codes and guidelines, such as ICC 500 (2014), FEMA (2015), and FBC (2017), introduce two types of missiles, i.e., small and large. The small missile is typically represented by a spherical steel ball, whereas the large missile is represented by a wood lumber projectile with the nominal cross-sectional dimensions of 50 mm × 100 mm (2 in. × 4 in.). In the existing literature, several studies have focused on the debris flight of compact objects (e.g., spheres) and sheet-type objects (e.g., roof shingles) (Tachikawa, 1983 and 1988; Wills et al., 2002; Holmes, 2004; Holmes et al., 2006; Baker, 2007; Visscher and Kopp, 2007; Kordi et al., 2010; Kordi and Kopp, 2011; Kakimpa et al., 2010 and 2012; Grayson et al., 2012; Baker

* Corresponding author.
E-mail addresses: dikshant@iastate.edu (D. Saini), shafei@iastate.edu (B. Shafei).

https://doi.org/10.1016/j.jweia.2022.105073
Received 17 December 2021; Received in revised form 22 May 2022; Accepted 19 June 2022

and Sterling, 2017; Uchibori and Tamura, 2019). However, only limited research has been devoted to the flight characteristics of rod-shaped objects, such as 2 × 4 lumbers.

As one of the first studies, Tachikawa (1988) experimentally investigated the free flight trajectories of both sheet- and rod-shaped debris objects. The referenced study indicated that the spread range increases with an increase in the aspect ratio of the debris. Later, Lin et al. (2007) examined the flight trajectories of rod-shaped objects by performing a set of tests in a wind tunnel with low turbulence characteristics. Although the experimental program consisted of various rod shapes, the investigation was limited to only two initial orientations, where the rods were placed along and across a uniform wind flow. Through wind tunnel tests, Richards et al. (2008) proposed a trajectory model with six degrees of freedom based on the aerodynamic coefficients measured for sheet- and rod-shaped debris objects at various pitch and yaw angles. Although the proposed model can be employed to determine the flight trajectory of roofing sheets and balsa rods, it requires a prior knowledge of the aerodynamic coefficients of the objects of interest in various orientations. In addition, it is important to note that a debris object interacts with its own wake and the eddies formed due to surrounding structures (Andersen et al., 2005). Such effects, which are known to be noticeable, particularly during debris take-off and early phases of flight, cannot be captured by the existing analytical models. To address the outlined issues and limitations, the presented study established a coupled computational fluid dynamics (CFD) and rigid body dynamics (RBD) simulation framework to obtain high-fidelity predictions of flight characteristics of rod-shaped debris objects, in the absence of any similar studies on this common type of debris.

With the increase of computational power over the past years, coupled CFD-RBD simulations have shown a great promise in determining the three-dimensional (3D) debris flight trajectories in space-related studies (Murman et al., 2005; Brown et al., 2006), as well as the studies focusing on wind events (Kakimpa et al., 2012; Saini and Shafei, 2021). For the purpose of the current study, the CFD-RBD simulation framework was designed to obtain the 3D motion of rod-shaped debris objects by the RBD solver using the flow data extracted from the CFD solver. Such a framework overcame the drawbacks of the existing computational methods, as it did not require any prior knowledge of debris aerodynamics. Therefore, a new capability was introduced to characterize the trajectories of different debris shapes/sizes and release conditions. In the presented manuscript, Section 2 outlines the details of the developed CFD-RBD simulation framework, along with the required assumptions. Section 3 provides the model validation studies performed to ensure the accuracy of predictions. Section 4 focuses on the free flight trajectories of rod-shaped debris objects in neutrally-stratified atmospheric boundary layer (ABL) winds. In particular, the referenced section covers various initial release conditions. Section 5 investigates the effects of a set of key influential factors, such as rod's geometry, initial orientation, and mean wind velocity, on debris flight characteristics. Finally, based on the wealth of simulation results collected, Section 6 introduces a series of predictive models to assess the kinetic energy associated with rod-shaped debris objects. Such models can be immediately used for the risk assessment of building envelopes, benefiting from the high-fidelity predictions of the travel distance and velocity of windborne debris objects.

2. Computational framework setup

This section presents a detailed description of the modeling details used for the wind flow surrounding the debris object, along with their interactions. The simulation framework developed to compute the flight trajectories of rod-shaped debris objects utilized ANSYS Fluent (2018). In the base CFD model, the wind flow was simulated inside a 3D rectangular domain that had an along-wind length of 80.0 m (in the x direction), cross-wind width of 30.0 m (in the z direction), and height of 30.0 m (in the y direction). Fig. 1 presents the main domain, in addition to the cross-section of the mesh generated around the rod object. For the benchmark simulation, a rod with a length of 900 mm and a rectangular section of 50 mm × 100 mm (2 in. × 4 in.) was considered. Given that the rod was assumed to be made of wood to replicate the lumber projectile, a total mass of 4.1 kg was assigned to it. Initially, the rod was positioned at 10.0 m from the inlet (in the x direction) and 15.0 m from the base surface (in the y direction), while its distance from each side wall was 15.0 m (in the z direction). With the rod flying in the 3D domain, the quality of mesh, i.e., skewness and aspect ratio, could be prone to deterioration. Specifically, the distortion of mesh close to the rod could have resulted in negative volume, leading to an early termination of the simulation. To preserve the mesh quality, following the modeling approach used by Kakimpa et al. (2012) and Saini and Shafei (2021), the rod-shaped object was placed in a non-deformable spherical region, which was coupled with the rod's motion. Outside the spherical region, however, was regularly re-meshed at each time step to ensure mesh quality. Upon completing a set of initial simulations, the size of the spherical region was decided to be 1.5 times of the rod's length.

The bottom surface of the simulation domain was modeled with a no-slip assumption. A roughness was also assigned to it, capturing the open terrain condition. The side walls were set as symmetric walls, which provided zero shear stresses. The left end and the top surface were modeled as velocity inlets. The flow profiles were assigned using a user-defined function for (i) mean wind velocity, (ii) turbulent kinetic energy, and (iii) turbulent energy dissipation. The right end, on the other hand, was modeled as a zero-gauge pressure outlet. The mesh discretization of the computational domain was achieved using a combination of structured and unstructured meshes. The spherical region was discretized using a structured mesh, while an unstructured mesh was developed outside of the spherical region. After completing a mesh sensitivity

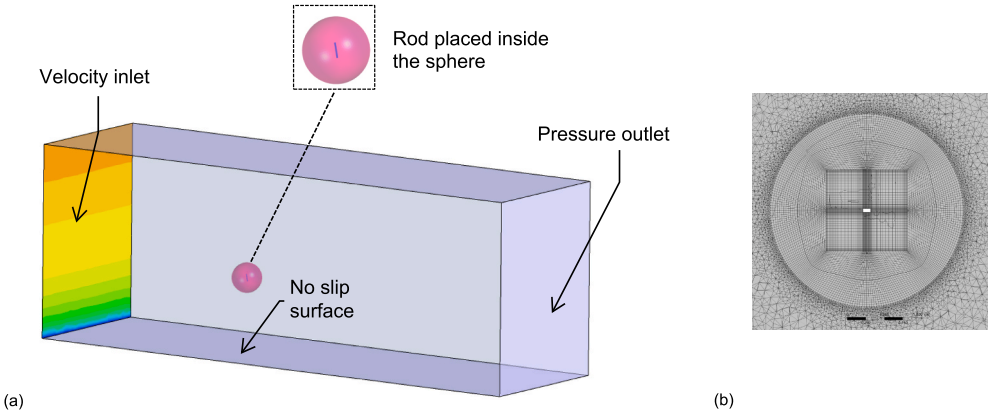

Fig. 1. (a) Details of the computational domain and associated boundaries, and (b) section cut through the computational domain showing the mesh pattern.

analysis, the entire domain was discretized to a set of 2.84×10^6 cells. In this study, the finite-volume method of Fluent (2018) was employed to utilize the unsteady incompressible Navier-Stokes model for capturing the flow field surrounding the rod-shaped debris object. Turbulence was modeled using a Realizable k-ε model with enhanced wall treatment. For the convection and viscous parts of the models, a second-order discretization method was utilized. In addition, a second-order interpolation was used for pressure from the centroid to the sides of each simulation cell.

The current study models the neutral ABL wind to further advance the state of the knowledge of debris flight characteristics for rod-shaped objects. In a study not related to debris flight, Richards and Hoxey (1993) proposed a method to simulate the ABL wind flow. Specifically, the following equations were employed in the developed simulation framework to model mean wind speed's vertical profile (U), kinetic energy of turbulence (k), and rate of turbulence dissipation (ε):

$$U(y) = \frac{u_*}{K_{\text{Karman}}} \ln\left(\frac{y + y_0}{y_0}\right) \tag{1}$$

$$k = \frac{u_*^2}{\sqrt{C_\mu}} \tag{2}$$

$$\varepsilon = \frac{u_*^3}{k(y + y_0)} \tag{3}$$

where u_* is the friction velocity; y_0 is the aerodynamic roughness length, which varies based on the terrain condition; y is the elevation above the ground; K_{Karman} is the von Karman's constant; and C_μ is the constant in the k-ε turbulence model, assumed equal to 0.09. For modeling the ground roughness at the bottom surface, the following expression was used to determine the equivalent sand roughness (κ_s):

$$\kappa_s = \frac{9.793 y_0}{C_s} \tag{4}$$

where C_s is the roughness constant taken as 0.5. From the initial simulations, it was observed that the conditions mentioned in Equations (1)–(4), in combination with the k-ε model, successfully produce the expected horizontal homogeneity of U, k, and ε for a neutral ABL wind.

In the 3D space, the rod's rigid body motion has six degrees of freedom, i.e., three translational and three rotational degrees of freedom about the three orthogonal axes. The rigid body motion of the rod-shaped debris can be defined using classical Newton-Euler equations, which consist of a series of six differential equations for six degrees of freedom. Thus, the following equations were used to define the movement of the rod-shaped debris objects:

$$m\left(\frac{d\vec{v}_{cg}}{dt}\right) + \vec{F}_g = \vec{F}_{cg} \tag{5}$$

$$\vec{I}_R \frac{d\vec{\omega}_R}{dt} = \vec{M}_R - \vec{\omega}_R \times \vec{I}_R \vec{\omega}_R \tag{6}$$

where m is the mass of the rod-shaped debris; $\vec{v}_{cg}$ is the translational velocity vector measured at the debris object's center of gravity; $\vec{F}_g$ is the gravitational force vector that acts on the debris object's center of gravity in the vertical downward direction; $\vec{F}_{cg}$ is the aerodynamic force vector that acts on the debris object's center of gravity; $\vec{I}_R$ is the moment of inertia's vector about the three orthogonal axes of the debris object; $\vec{\omega}_R$ is the angular velocity vector; and $\vec{M}_R$ is the aerodynamic moment vector.

The coupled CFD-RBD simulations were conducted in two stages. In the first stage, unsteady Reynolds-averaged Navier-Stokes (RANS) simulations were performed without the dynamic movement of debris to allow the development of the expected flow. After the flow was developed, the debris was released in the wind flow. At each time step, the RBD solver calculated the dynamic movement of the debris based on the pressure forces and moments obtained from the CFD solver. Depending on the movement of the debris, the mesh of the computational domain was updated prior to the next time step. At each time step, the movement of the debris was recorded, in terms of translational and angular components.

3. Model validation and investigations under uniform wind flows

To ensure the reliability of the developed simulation framework, rigorous validation studies were performed using the information available in the literature. In the first step, a series of simulations were conducted to replicate the flight trajectory of a balsa rod recorded from the wind tunnel experiments (Richards et al., 2008). In the experiments, a balsa rod with a cross-section of 10 mm × 10 mm and a length of 200 mm had been considered. Under a uniform wind flow, the rod was released along the wind flow with a pitch angle of 0°. Fig. 2 shows how the rod's angular displacements have been defined for the current study. In the referenced figure, B is the rod's dimension measured in the cross-wind direction, D is the rod's dimension measured in the vertical direction, and L is the rod's dimension in the along-wind direction. The computational domain was modeled as a 7.0 m × 2.0 m × 2.0 m box, consistent with the wind tunnel test setup. An average cell size of $D/20$ was used at the vicinity of the rod. In the regions away from the rod, the

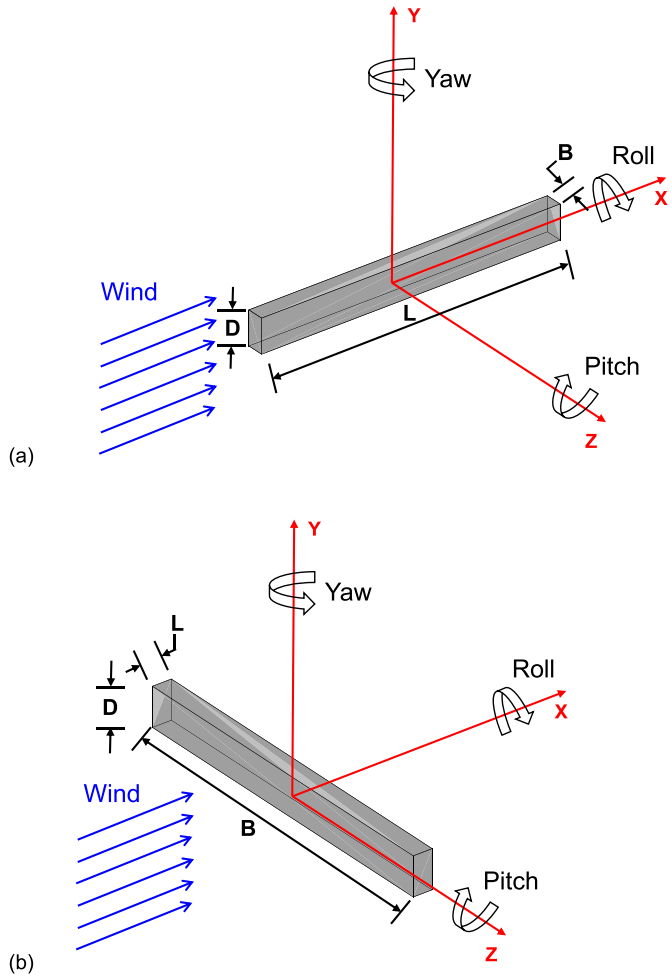

Fig. 2. A schematic sketch of the rod's angular movements in the wind flow: (a) the rod placed in the along-wind direction, and (b) the rod placed in the across-wind direction. The presented rods have an initial pitch angle of 90°. The pitch angles are measured in the clockwise direction.

mesh size was gradually increased. The spherical region was modeled with a diameter equal to the twice of the rod's length. Further away from the spherical region, the outside domain was modeled with a maximum cell size of 0.2 m. Fig. 1(b) shows a typical mesh pattern developed for the coupled CFD-RBD model. The rod was kept at 1.5 m from the inlet (i.e., in the x direction). For modeling the flow field, following the wind tunnel experiments, a uniform wind velocity of 9.1 m/s was applied to the inlet with a turbulence intensity of 2.0% and a length scale of 0.01 m. The rod was kept in its initial orientation for 250 msec to allow the formation of the flow field around it. After that, the rod was released in the wind and the free flight trajectories were extracted by calculating the translational and angular components. Fig. 3 compares the flight trajectory of the balsa rod when it was released along the wind flow. By comparing the computed results to the wind tunnel test data, it was noted that the developed simulation framework can produce free flight trajectories consistent with those from the experiments.

The validation effort was then further extended by calculating the free flight trajectories of a rod-shaped object with the cross-sectional dimensions of 50 mm × 100 mm and a length of 900 mm. This rod size well represents the 2 × 4 lumber projectiles separated from buildings during extreme wind events. Studies focusing on the flight trajectories of rod-type objects are scarce in the existing literature. Lin et al. (2007) conducted wind tunnel tests on the scaled models of 2 × 4 rods released in a uniform wind flow. The debris models included in the wind tunnel tests consisted of 8 rods released in two initial orientations, i.e., along and across the wind flow. For each orientation, the rods were released at the pitch angles of 0°, 15° and 45°. Using the test results, Lin et al. (2007) provided mean fit equations to predict the horizontal distance and velocity of rod-shaped debris objects. For validation purposes, the referenced wind tunnel tests were replicated in the current study and the outcome was compared to the mean fit equations proposed by Lin et al. (2007) for the cross-wind and along-wind directions, as expressed in Equations (7) and (8), respectively:

$$Kx^* \approx 0.4005(Kt^*)^2 - 0.160(Kt^*)^3 + 0.036(Kt^*)^4 - 0.0032(Kt^*)^5 \quad (7)$$

$$Kx^* \approx 0.4005(Kt^*)^2 - 0.294(Kt^*)^3 + 0.088(Kt^*)^4 - 0.0082(Kt^*)^5 \quad (8)$$

where Kx^* is the non-dimensional horizontal distance ($= Kxg/U^2$); Kt^* is the non-dimensional time ($= Ktg/U$); and K is the Tachikawa number.

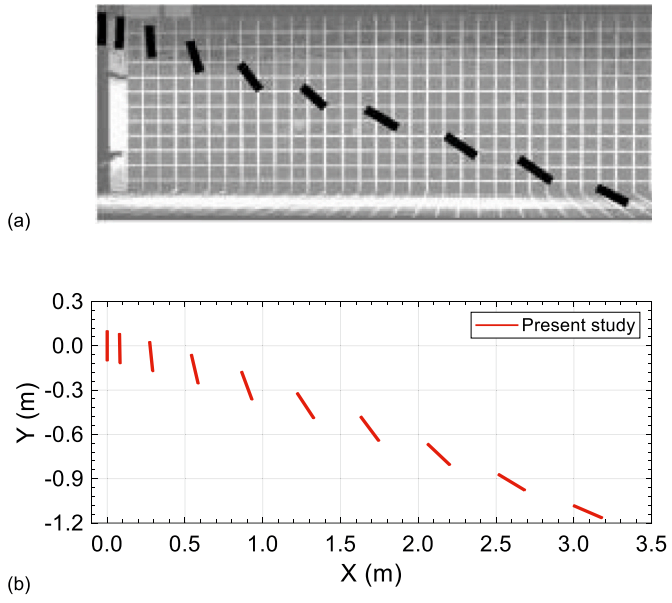

Fig. 3. Comparison of the free flight trajectory of 10 mm × 10 mm × 200 mm balsa rod in a wind speed of 9.1 m/s: (a) images captured by Richards et al. (2008), and (b) simulation results.

The Tachikawa number can be calculated by Equation (9):

$$K = \frac{\rho U^2 A}{2mg} \quad (9)$$

where ρ is the air density taken as 1.225 kg/m^3; A is the largest surface area of the rod, i.e., 0.1 m × 0.9 m in the current validation study; m is the rod's mass, equal to 4.1 kg; U is the rod's mean wind velocity; and g is the gravitational acceleration, equal to 9.81 m/s^2.

The coupled CFD-RBD model was developed based on the procedure defined in Section 2. From the preliminary investigations on the drag and lift coefficients of the rod-shaped objects, a mesh size of $D/40$ was decided at the vicinity of the rod. To minimize the computational demand, the mesh size was increased gradually outside the spherical region, following the details explained for the first validation study. From the time sensitivity analysis, a time step of 0.002 s was determined to be appropriate for obtaining the results independent of time step. The flight trajectories of the 2 × 4 rod were simulated for two rod orientations, i.e., in the along-wind and cross-wind directions. For both orientations, the flight trajectories were calculated for two wind velocities of 20 m/s and 30 m/s, further to five pitch angles, ranging between 0° and 90° (at an interval of 22.5°). For the two wind velocities of 20 m/s and 30 m/s, the Tachikawa number (K) was calculated to be 0.55 and 1.23, respectively. The investigations were conducted in a flow condition resembling that of the low-turbulence wind tunnel. For this purpose, the wind speed was applied to the inlet, assuming a turbulence intensity of 2% and a length scale of 0.1 m. For all the simulations, the rod was kept in its initial position for 2.5 s to develop the flow field around it. The flight trajectories were recorded, in terms of translational and angular components, as a function of flight time.

Figs. 4 and 5 show the flight trajectories for initial pitch angles, ranging from 0° to 90° (in 22.5° intervals) when the rod was released in the along-wind and cross-wind directions, respectively. Consistent with the experiments conducted by Lin et al. (2007), the rod's flight trajectories were found to be influenced by the initial pitch angle. In the case of rods released along the wind flow, the equation proposed by Lin et al. (2007) was noted to be in the range but overall underestimated the flight trajectories compared to those from the CFD-RBD simulations (Fig. 4(a)). A similar situation was observed in the velocity profiles (Fig. 4(b)). On the other hand, for the rods released across the wind flow, the expression proposed by Lin et al. (2007) was found to overestimate the trajectories compared to those obtained from the CFD-RBD simulations (Fig. 5(a) and (b)). This can be explained by the fact that the experiments performed by Lin et al. (2007) consisted of scaled rod models with lengths between 330 mm and 380 mm, weighing between 5.5 g and 17.9 g. This resulted in Tachikawa numbers between 3.8 and 27.7, which were significantly higher than those of the representative rod used in the current simulations. In addition, the L/B ratio in the experiments conducted on the rods in the along-wind direction was between 26.0 and 30.0. However, the L/B ratio for the 2 × 4 lumber projectile investigated in this study was 9.0. Despite the discussed deviations and supporting reasons, the trajectories extracted from the CFD-RBD simulations were observed to be comparable to those reported by Lin et al. (2007), in terms of both magnitude and trend. Thus, based on the outcome of these detailed model validation studies, it was concluded that the developed simulation framework can properly predict the flight trajectories of rod-shaped debris objects.

4. Flight characteristics of rod-shaped debris in ABL wind flows

The flight characteristics of a rod with a cross-section of 50 mm × 100 mm and a length of 900 mm were investigated under the ABL wind. For this purpose, two initial orientations were considered, i.e., in the along-wind and cross-wind directions. In the first set of simulations, the debris for each orientation was released in the wind flow at various initial pitch angles, ranging between 0.0° and 157.5° (at an interval of

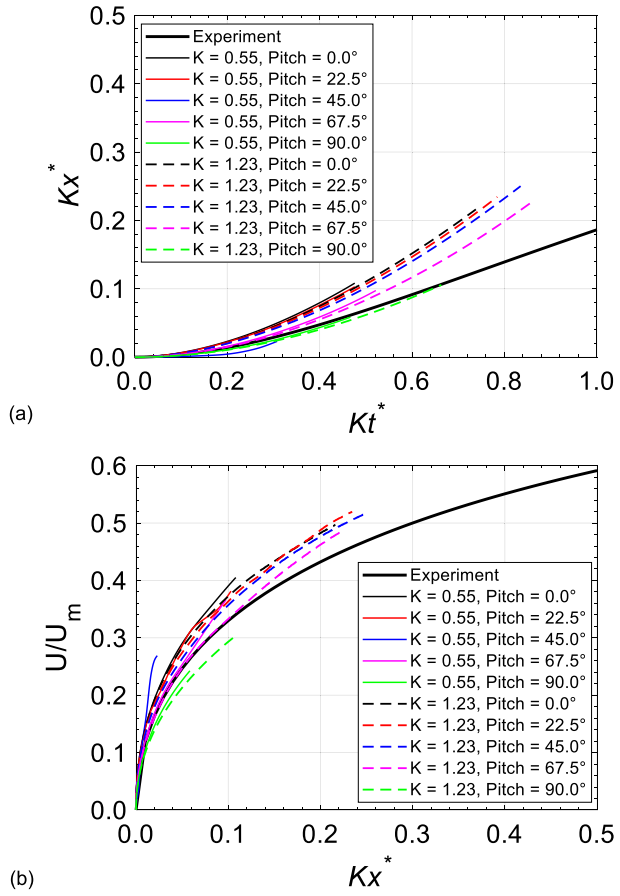

Fig. 4. Mean flight trajectories obtained for the rod released in the along-wind direction with a range of initial pitch angles from 0.0° to 90°: (a) comparison of the recorded non-dimensional horizontal displacements to those reported in Lin et al. (2007), and (b) comparison of the recorded non-dimensional horizontal velocities to those reported in Lin et al. (2007).

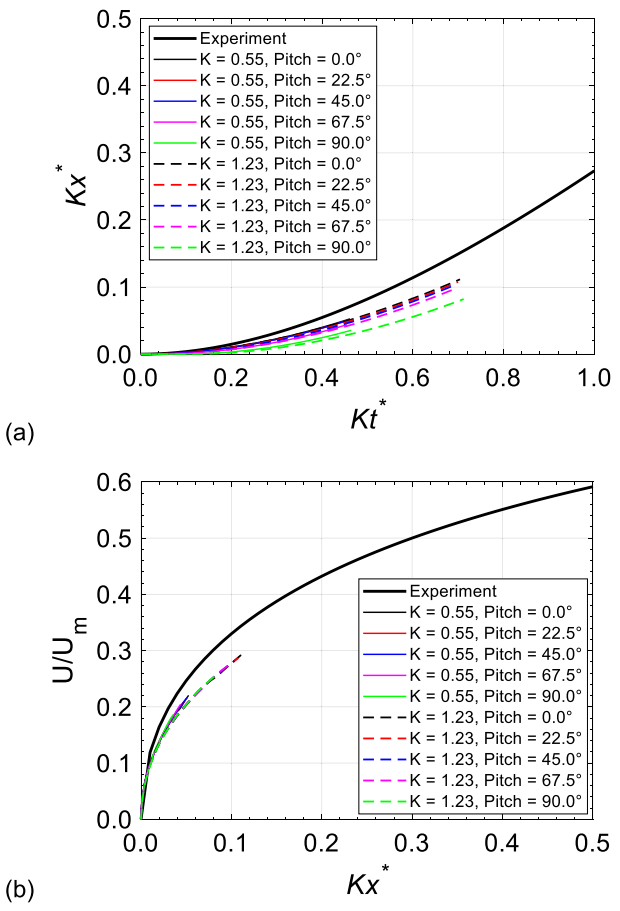

Fig. 5. Mean flight trajectories obtained for the rod released in the cross-wind direction with a range of initial pitch angles from 0.0° to 90°: (a) comparison of the recorded non-dimensional horizontal displacements to those reported in Lin et al. (2007), and (b) comparison of the recorded non-dimensional horizontal velocities to those reported in Lin et al. (2007).

22.5°). To allow the formation of flow field around the debris, the rod was held in its initial orientation for 2.0 s. Fig. 6 presents the 3D flow structures developed using the Q-criterion in the wake of the rod that had been released with a pitch angle of 135°. The flow structure consisted of edge vortices, which created an asymmetric distribution. The shedding of the vortices from the rod's tips caused the rod to rotate with an increased angular velocity. This is also evident in the flight trajectories captured in Fig. 7, where the rods are found to rotate more in the ABL wind than in the uniform flow. For each simulation, the rod's free flight trajectory was computed by recording the translational and angular components. To further evaluate the effects of the ABL wind flow on the free flight trajectories of rod-shaped debris objects, the displacement and velocity profiles were directly compared to those extracted from the uniform wind flow. Fig. 7 presents the rod's flight trajectories in the uniform and ABL wind flows, considering the initial pitch angles of 0°, 22.5°, 45.0°, and 67.5°. In both wind regimes, the rod was released along the wind flow from a height of 15.0 m. The mean wind velocity at the release height was 30.0 m/s (equivalent to a Tachikawa number of 1.23).

With plotting the rod's position in the *x*-*y* plane every 100 msec, Fig. 7 clearly shows that the recorded flight trajectories were significantly affected by taking into consideration the ABL wind properties. At the initial pitch angle of 0°, the rod in the ABL wind traveled a shorter distance than that in the uniform wind. With increasing the initial pitch angle to 22.5°, 45.0°, and 67.5°, the deviation of travel distance between ABL wind and uniform wind increased further. This can be explained by differences in the lift forces that the rod-shaped object experienced in the ABL and uniform winds. After release, the rod started a downward movement. In case of ABL wind, however, the mean wind velocity reduced with the drop of elevation. This caused the rod to travel a shorter distance in the ABL wind than in the uniform wind. This situation was magnified with increasing the pitch angle, as captured in Fig. 7 (a) through 7(d). In the next step, the ABL wind effects on the rod's flight trajectories were investigated using the horizontal (U), vertical (V), and angular velocity (ω_z) components. Fig. 8 compares the velocity components of the rod released with the initial pitch angles of 22.5° and 67.5° in the ABL and uniform wind flows. For both initial pitch angles, the vertical velocity was observed to be higher in the ABL wind than in the uniform wind. Therefore, the horizontal distance that the rod traveled in the ABL wind was shorter than that in the uniform wind. Among the three velocity components, the angular velocity components witnessed the most significant difference marked by oscillation in their profiles.

The flight trajectories of rod-shaped debris objects were observed to have significant differences from those recorded for plate-shaped objects. In a separate investigation, Saini and Shafei (2021) reported that plates can achieve a horizontal velocity approximately equal to the mean wind velocity. This, however, was not the case for rods, owing to their higher mass and lower surface area. The outlined observation was further confirmed based on the lower drag and lift forces recorded for rods compared to plates. To obtain a holistic perspective, the horizontal and vertical distances traveled by rod-shaped debris objects were studied further in the ABL wind. For the pitch angles between 0° and 157.5°,

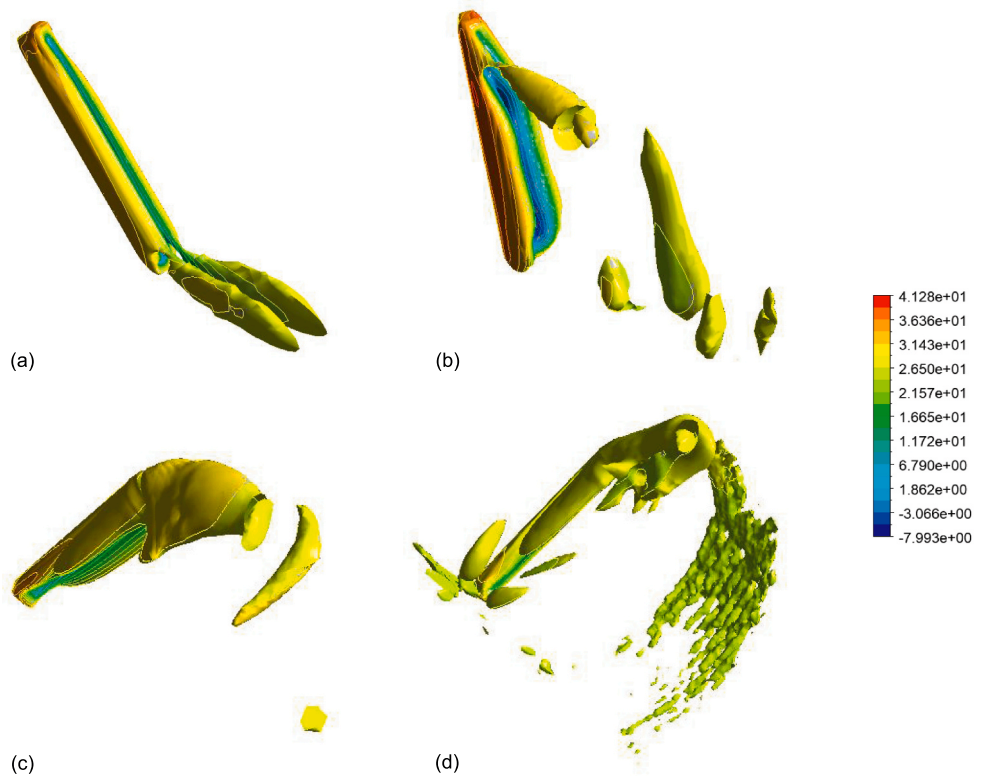

Fig. 6. Instantaneous iso-surfaces of Q-criterion colored by velocity magnitude (m/s) around the rod released in the along-wind direction of ABL flow fields (with an initial pitch angle of 135°) after (a) 0.0 s, (b) 0.5 s, (c) 1.5 s, and (d) 2.0 s.

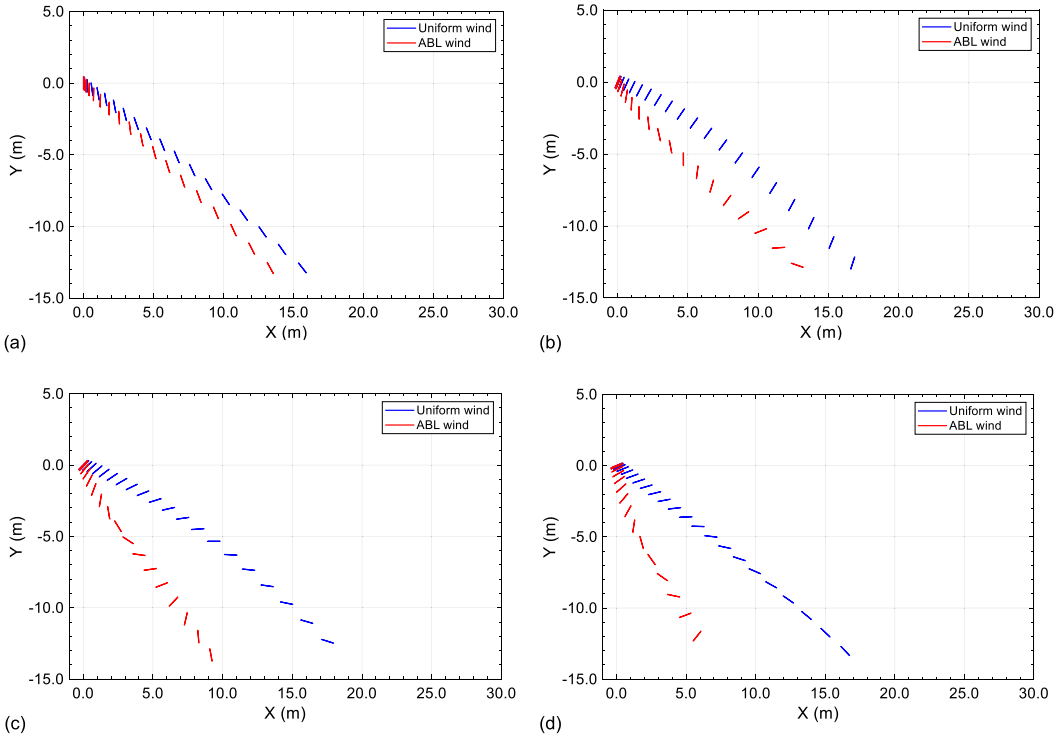

Fig. 7. Comparison of the flight characteristics for the rods released in the along-wind direction under the uniform and ABL winds with an initial pitch angle of (a) 0.0°, (b) 22.5°, (c) 45.0°, and (d) 67.5°.

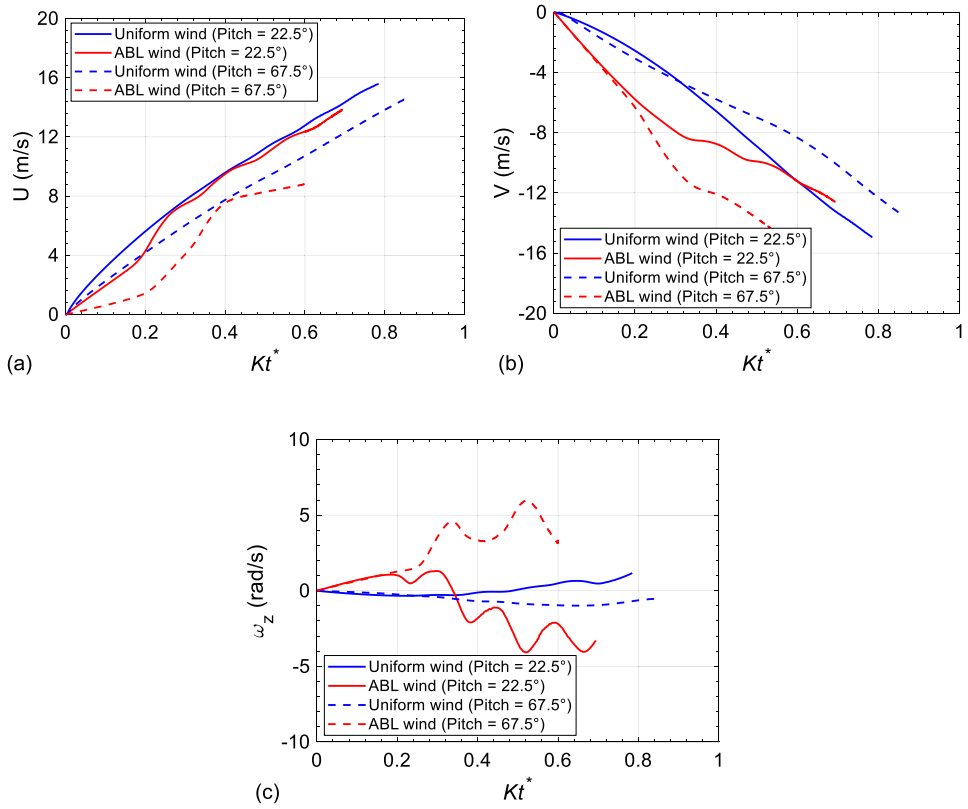

Fig. 8. Comparison of the rod's velocity components for two initial pitch angles of 22.5° and 67.5° in the uniform and ABL wind flows: (a) horizontal velocity, (b) vertical velocity, and (c) angular velocity.

Fig. 9 presents the rod's free flight trajectories, in terms of non-dimensional horizontal and vertical distances, as a function of non-dimensional time. The rod's initial orientation was determined to significantly influence the obtained distributions. Specifically, the horizontal distance that the rod traveled was noted to be minimum when the rod's longitudinal axis was placed along the wind flow, i.e., a pitch angle of 90°. Fig. 9(b) shows that the rod tended to move downward for all pitch angles. Specifically, despite an initial upward movement for the pitch angles greater than 90°, the lift forces were not enough to move the rod above its initial position. This was different from the plate-shaped debris objects, which were found to experience an upward movement, depending on the initial pitch angle.

5. Investigation of key influential factors

To study the key factors that affect the flight characteristics of rod-shaped debris objects, a series of CFD-RBD simulations were performed with a focus on the following parameters: (i) mean wind velocity, (ii) rod's length to depth ratio (L/D), (iii) rod's width to depth ratio (B/D), and (iv) rod's initial orientation with respect to the wind flow. For each of the selected factors, a wide range of pitch angles, i.e., between 0° and 157.5° (with an interval of 22.5°), were simulated. The simulations performed to capture the effect of mean wind velocity covered three mean wind velocities of 30 m/s, 40 m/s, and 50 m/s. The listed velocities were defined at the elevation of 15.0 m, where the rod was released. The Tachikawa numbers calculated for these three velocities were 1.23, 2.19, and 3.43, respectively. For this set of investigations, all the simulations were conducted using a rod with a cross-section of 50 mm × 100 mm, a length of 900 mm, and a mass of 4.1 kg. Fig. 10 presents the horizontal and vertical distances that the rod object traveled over time. The obtained profiles show that the horizontal and vertical distance traveled by the rod were both affected by the mean wind velocity. In particular, for the mean wind velocity of 50.0 m/s, the rod was observed to experience lift forces. This was further studied by making a side-by-side comparison of the debris flight profiles, as shown in Fig. 11. While the rod subjected to the mean wind velocity of 30.0 m/s had a straight-line trajectory, the trajectory started to show a nonlinear profile, as the mean wind velocity increased to 50.0 m/s. This observation was further confirmed by noting that the flight trajectory depends on the Tachikawa number.

To evaluate the effect of the debris length on flight trajectories, the rod object considered in the current study was modified. For this purpose, the cross-sectional dimensions were kept unchanged, representing those of 2 × 4 lumber projectiles. However, three new rod lengths, i.e., 600 mm ($L/D = 6.0$), 750 mm ($L/D = 7.5$), and 1200 mm ($L/D = 12.0$), were introduced, in addition to the base case, which had a length of 900 mm ($L/D = 9.0$). The simulations were conducted for a mean wind velocity of 40 m/s at the release height of 15.0 m for all the cases. The Tachikawa number remained the same for all the four rods, i.e., 2.19. This was because the change of length proportionally changed the mass as well. Fig. 12 presents the flight trajectories of the four rod objects released with the two pitch angles of 45° and 135°. The obtained trajectories showed how the rod's length affects the trajectories. Despite the fact that no notable difference was observed in the flight trajectories for the pitch angle of 45°, the difference became apparent for the pitch angle of 135°. The next parameter examined was the rod's width to depth ratio (B/D ratio). In addition to the B/D ratio of 0.50 considered for the base case, two additional rod shapes with the B/D ratios of 0.25 and 0.75 were investigated. For this purpose, the depth was maintained at 50 mm, while the width was changed. The simulations were conducted in the ABL wind, assuming a mean wind velocity of 40 m/s at the release height of 15.0 m for all the cases. With the change in the rod's width, the mass also proportionally changed, resulting in a range of Tachikawa numbers. Specifically, the Tachikawa numbers calculated for

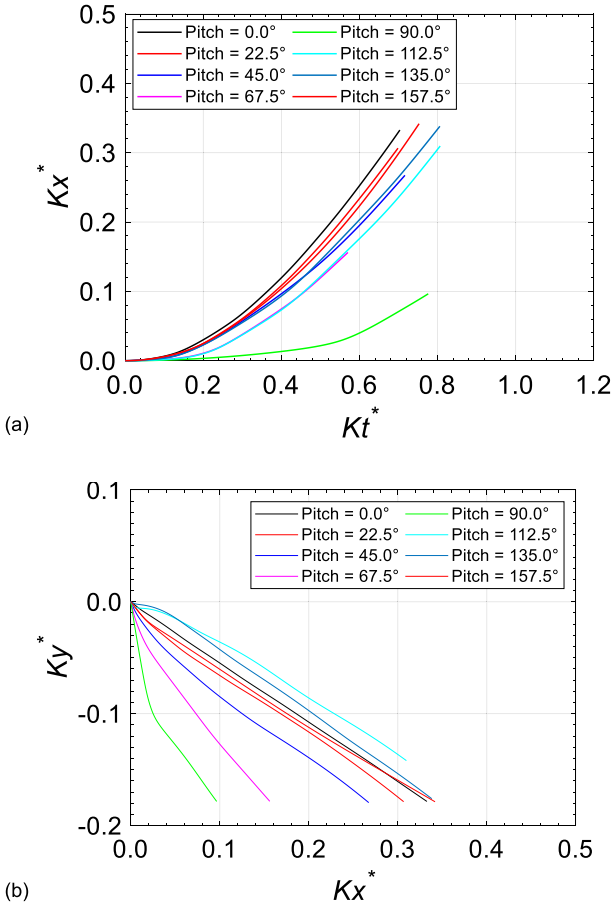

Fig. 9. Mean flight trajectories obtained for the rod released in the along-wind direction with various initial pitch angles: (a) non-dimensional horizontal distance versus non-dimensional time, and (b) non-dimensional vertical distance versus non-dimensional horizontal distance.

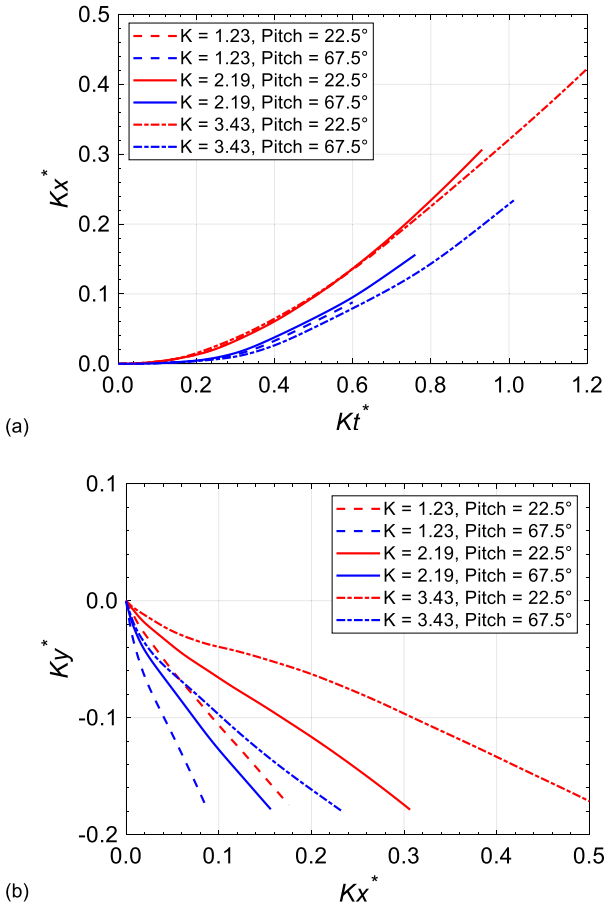

Fig. 10. Effect of mean wind velocity on the flight trajectories recorded for the rod released in the along-wind direction: (a) horizontal distance as a function of time, and (b) vertical distance as a function of horizontal distance traveled by the rod.

the rods with the *B/D* ratios of 0.25, 0.50, and 0.75 were 4.38, 2.19, and 1.46, respectively. Fig. 13 presents a side-by-side comparison of how the rods with different *B/D* ratios fly, assuming an initial pitch angle of 45°. The rod with the highest Tachikawa number, i.e., *B/D* ratio of 0.25, traveled farthest. With increasing the *B/D* ratio, the rod object witnessed more rotation, which correlated well with the fact that the rod was traveling at a lower horizontal velocity. The horizontal distance that the rod traveled also consistently increased with decreasing the *B/D* ratio.

The last parameter studied in this section was the rod's initial orientation. In the previous simulations, the rod had been placed in the along-wind direction. To investigate the consequences of debris orientation, a second orientation was considered in which the rod's longitudinal axis was placed in the cross-wind direction, as reflected in Fig. 2 (b). All the simulations were conducted in the ABL wind, assuming a mean wind velocity of 40.0 m/s at the release height of 15.0 m. To obtain an in-depth understanding of flight trajectories, the flow structure was first analyzed at regular time intervals during the flight. Fig. 14 presents the 3D flow structures developed using the Q-criterion in the wake of the rod placed across the wind flow with an initial pitch angle of 90°. This figure captured tip vortices at the time of release. As the rod started moving forward, the tip vortices were combined with leading and trailing edges. Fig. 14(c) and (d) showed that the interaction between the vortices led to a weak shedding of the vortices. In contrast to the rod placed in the along-wind direction, a symmetric flow structure was observed for the rod placed in the cross-wind direction. This eliminated the magnification of the rod's angular velocity, as observed when the rod was released in the along-wind direction. The flight trajectories of the rod placed in the cross-wind direction were further studied for the three pitch angles of 0.0°, 45.0°, and 90.0°. Fig. 15 presents the mean flight trajectories, in terms of the horizontal distance traveled by the rod and its corresponding horizontal velocity. The initial pitch angle was determined not to be a dominant factor as similar trajectories were obtained for the investigated pitch angles. This was in contrast to the trajectories obtained for the rod placed in the along-wind direction.

6. Prediction of flight trajectories

To perform a wind hazard analysis that involves windborne debris impact, it is critical to predict the possible impact location and corresponding impact energy (Saini and Shafei, 2020a,b; Kulkarni and Shafei, 2021). The impact location can be directly determined by computing the debris flight trajectory, while the debris velocity can be employed to assess the impact kinetic energy. This study investigated the flight trajectories of rod-shaped debris objects with a wide range of geometric properties, initial release conditions, and flow regimes. Therefore, the original data generated from this study was further utilized to develop the predictive equations that capture the horizontal travel distance and velocity of rod-shaped objects during their flights. Because of flight complexities, both the horizontal distance and velocity were observed to have notable variations, as also reported by Lin et al. (2007). Thus, the horizontal trajectories were presented as a function of non-dimensional horizontal distance versus non-dimensional time. Based on the collected data points, Equation (10) was found to predict the mean trajectory of rod-shaped debris objects:

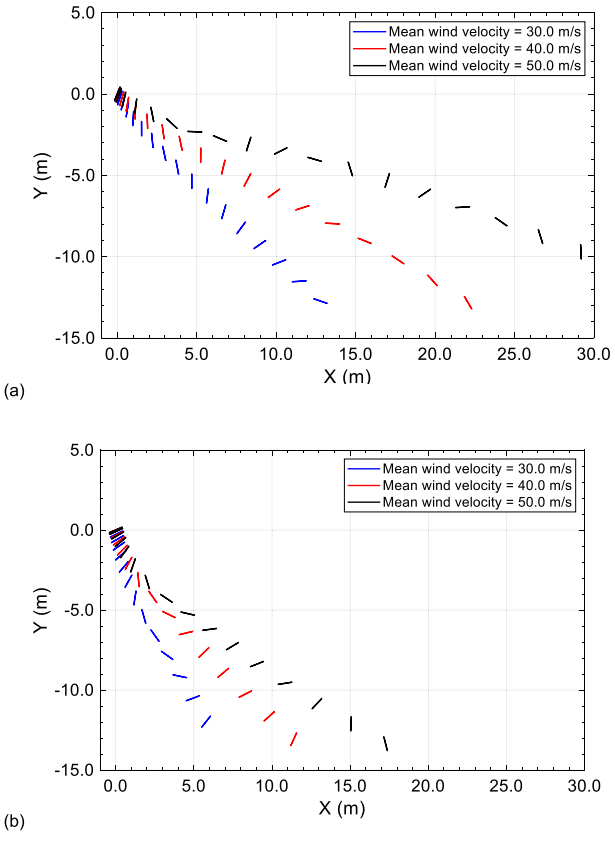

Fig. 11. Recorded flight trajectories in various mean wind velocities for the two initial pitch angles of (a) 22.5°, and (b) 67.5°.

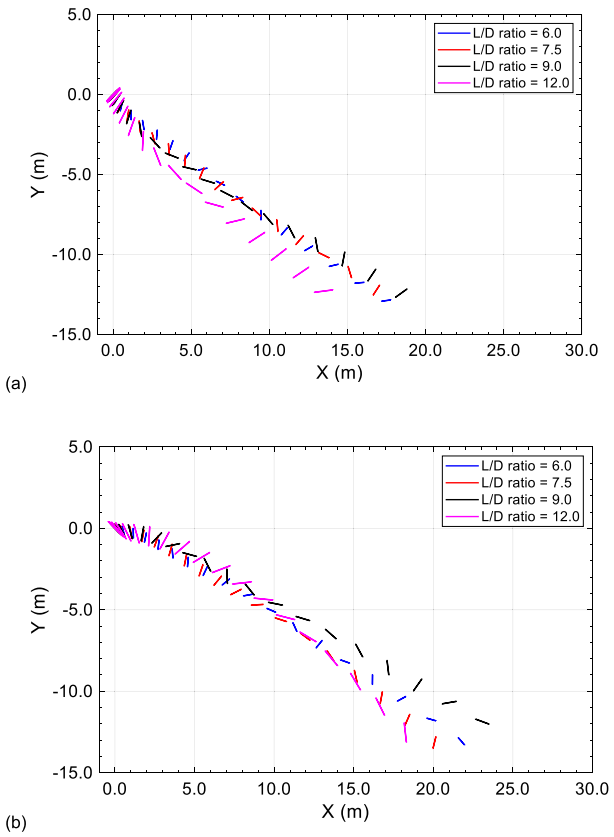

Fig. 12. Mean flight trajectories of the rods with four different *L/D* ratios released with the two initial pitch angles of (a) 45.0°, and (b) 135.0°.

$$Kx^* = \frac{-0.141Kt^{*3} + 0.803Kt^{*2} - 0.1489Kt^* + 0.006}{Kt^* + 0.85} \tag{10}$$

Fig. 16(a) shows the mean equation fitted, in addition to the 95% confidence intervals. The prediction bounds included in the referenced figure capture variations in recorded debris flight trajectories. This was computed using the inverse of the Student's *t* cumulative distribution function. Since the kinetic energy is required to estimate the loading demand induced to building envelopes by impacting windborne debris, the horizontal velocities obtained from the simulations were utilized as well. For this purpose, the recorded horizontal velocities were normalized by U_H, where U_H is the mean wind velocity recorded at the debris release point. Fig. 16(b) shows the non-dimensional horizontal velocity for a range of rod objects and flow conditions. From the data generated during the simulations, Equation (11) was derived to predict the horizontal velocity of rod-shaped debris objects:

$$U \Big/ U_H = 0.840(1 - e^{-\sqrt{3.015Kx^*}}) \tag{11}$$

The combination of Equations (10) and (11) can predict the kinetic energy of rod-shaped debris objects in the ABL wind. The obtained predictive models are expected to assist with the evaluation of the likelihood and energy of windborne debris impact, especially where the rod-shaped objects are the dominant type of debris.

7. Conclusions

The presented study explored the flight trajectories of rod-shaped debris objects in the ABL wind flow. Considering that the relevant literature was limited in scope and only focused on the flight characteristics of rod-shaped objects in the uniform wind, the current study developed a high-fidelity CFD-RBD simulation framework to capture the flight trajectories of various rods released with a wide range of initial orientations. Appropriate validation studies were first performed to ensure the accuracy of predictions. The developed simulation framework was then utilized to compute the flight trajectories of lumber projectiles commonly observed in the extreme wind events. The outcome was reported, in terms of horizontal and vertical distances traveled by the debris, further to the linear and angular velocities that the debris experienced. The simulation matrix was then extended to cover the effects of several influential factors, including mean wind velocities, rod's length to depth ratio, rod's width to depth ratio, and initial orientation. The following main conclusions were drawn from this study:

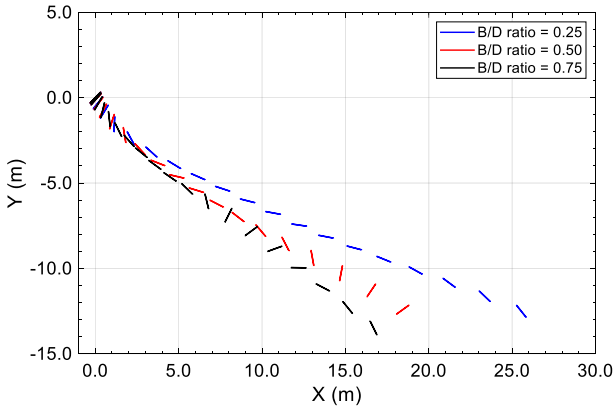

Fig. 13. Effect of *B/D* ratio on the mean flight trajectories of the rods released with an initial pitch angle of 45°.

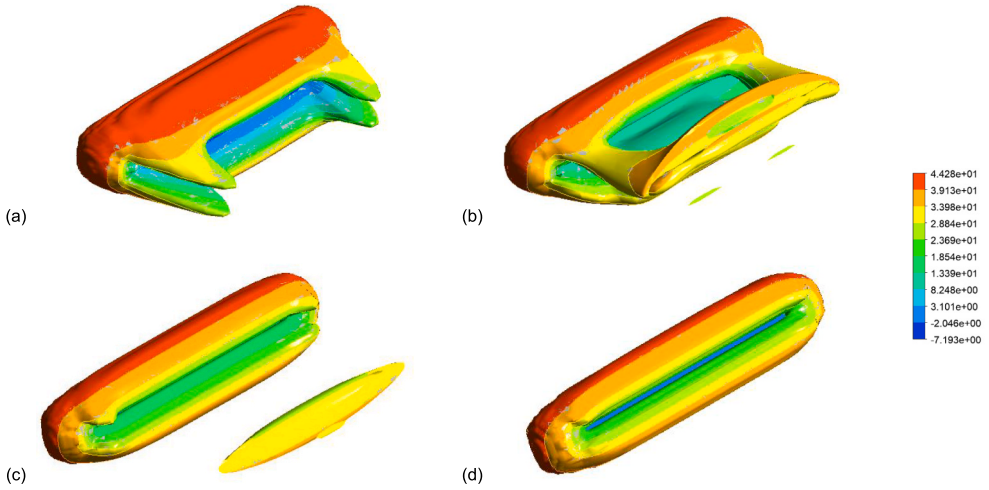

Fig. 14. Instantaneous iso-surfaces of Q-criterion colored by velocity magnitude (m/s) around the rod released in the cross-wind direction of ABL flow fields (with an initial pitch angle of 90°) after (a) 0.0 s, (b) 0.5 s, (c) 1.5 s, and (d) 2.0 s.

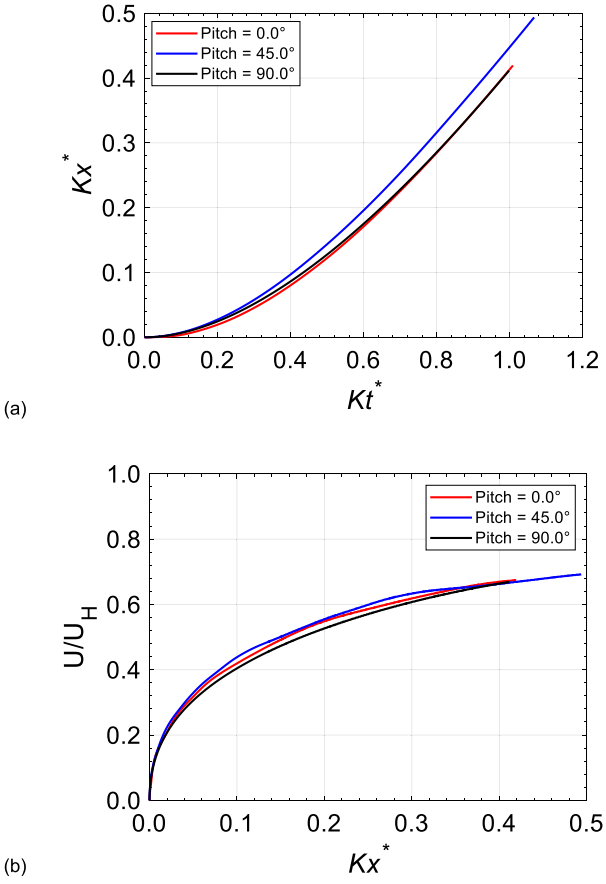

Fig. 15. Mean flight trajectories obtained for the rod released in the cross-wind direction with three initial pitch angles of 0.0°, 45.0°, and 90.0°: (a) non-dimensional horizontal displacement versus time, and (b) normalized horizontal velocity as a function of non-dimensional horizontal displacement.

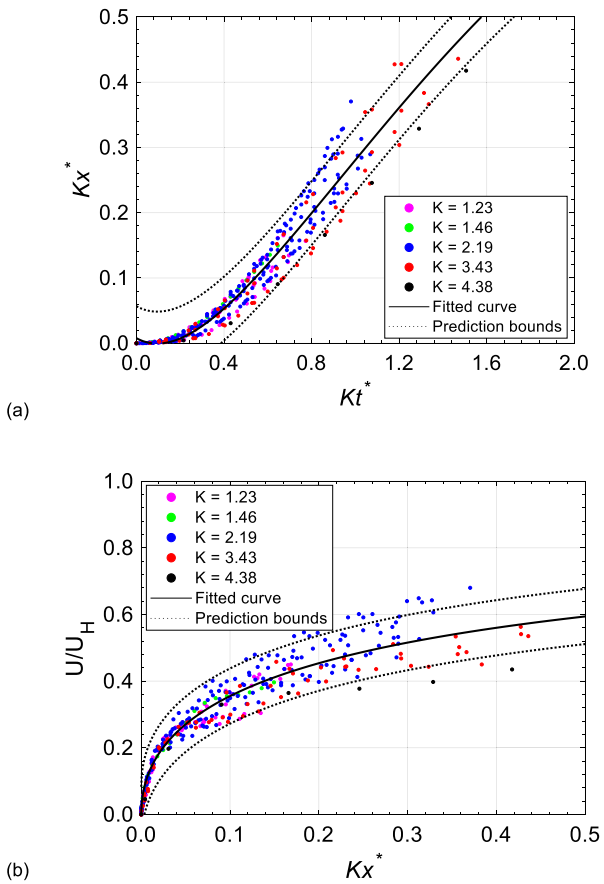

Fig. 16. (a) Non-dimensional horizontal trajectories of the rod-shaped debris objects as a function of non-dimensional time, and (b) normalized horizontal velocity versus non-dimensional horizontal travel distance.

- Focusing on the flight trajectories of rod-shaped objects, it was revealed that the distance traveled by the debris can differ significantly, depending on the wind regime. Specifically, the rods were noted to travel a shorter distance in the ABL wind than in the uniform wind for the range of pitch angles investigated. This was attributed to the lower drag and lift forces in the ABL wind, in contrast to those in the uniform wind.
- From the comparison of the flight trajectories of rod-shaped debris objects with those of plate-shaped debris objects, it was observed

that the rod's velocity never reached (or exceeded) the mean wind velocity, in contrast to plates. This was primarily due to the fact that plates (owing to their larger surface areas) experience significant lift forces compared to rods. As a result, rods did not move in the upward direction above their initial positions.

- The investigations on the effect of mean wind velocity revealed that a complex flight pattern, including notable rotations, can be created for high mean wind velocities. Specifically, a linear trajectory was recorded for the rod under the mean wind velocity of 30 m/s. However, the rod trajectory became nonlinear when the mean wind velocity increased to 50 m/s. This highlighted the importance of Tachikawa number, as the rods with a higher Tachikawa number traveled faster and farther than those with a lower Tachikawa number.
- The effect of rod's length to depth ratio was investigated by changing the length of the lumber projectile. This consisted of four rods with the length to depth ratios of 6.0, 7.5, 9.0, and 12.0. The Tachikawa number remained the same for all the four rods, as the rod's mass changed proportional to its length. Although the difference in the trajectory pattern was not significant, the distance traveled by the rods varied.
- The investigations on the effect of rod's width to depth ratio were conducted by varying the width of the rod, generating a range of ratios, i.e., 0.25, 0.50, and 0.75. Change in the rod's width to depth ratio proportionally changed the Tachikawa number. The horizontal distance that the rods traveled consistently increased by decreasing their width to depth ratio. Further to the changes recorded in the travel distance, the rods showed considerably more rotations with the increase of their width to depth ratio.
- Based on the wealth of data obtained from the CFD-RBD simulations, the current study developed two predictive models to estimate the mean horizontal distance traveled by rod-shaped debris objects and their corresponding mean horizontal velocity. This was paired with 95% confidence intervals to provide the input necessary for the assessment of building envelopes prone to the windborne debris hazard.

CRediT authorship contribution statement

Dikshant Saini: Methodology, Software, Validation, Investigation, Writing – original draft. **Behrouz Shafei:** Conceptualization, Methodology, Investigation, Writing – review & editing, Supervision, Funding acquisition.

Declaration of competing interest

The authors declare that they have no known competing financial interests or personal relationships that could have appeared to influence the work reported in this paper.

Acknowledgement

The research study, results of which reported in this manuscript, was partially sponsored by the National Science Foundation (NSF) under Grants No. 1826356 and 2125426. The authors would like to acknowledge and thank the sponsor for this support. Opinions, findings, and conclusions expressed in this manuscript are of the authors and do not necessarily reflect those of the NSF.

References

Andersen, A., Pesavento, U., Wang, Z.J., 2005. Unsteady aerodynamics of fluttering and tumbling plates. J. Fluid Mech. 541, 65–90.
Baker, C.J., 2007. The debris flight equations. J. Wind Eng. Ind. Aerod. 95, 329–353.
Baker, C.J., Sterling, M., 2017. Modelling wind fields and debris flight in tornadoes. J. Wind Eng. Ind. Aerod. 168, 312–321.
Brown, J., Bogdanoff, D., Yates, L., Wilder, M., Murman, S., 2006. Complex-trajectory aerodynamics data for code validation from a new free-flight facility. Proc. 44th AIAA Aero. Sci. Meet. Exhibit. 1–15.
FBC (Florida Building Commision), 2017. Florida Building Code. Tallahassee, FL.
FEMA, 2011. Coastal Construction Manual: Principles and Practices of Planning, Siting, Designing, Constructing, and Maintaining Residential Buildings in Coastal Areas (FEMA P-55). Federal Emergency Management Agency, Washington, DC.
FEMA, 2015. Safe Rooms for Tornadoes and Hurricanes: Guidance for Community and Residential Safe Rooms (FEMA P-361). Federal Emergency Management Agency, Washington, DC.
Fluent, 2018. ANSYS Fluent Theory Guide, 19.2. ANSYS, Canonsburg, PA.
Grayson, M., Pang, W., Schiff, S., 2012. Three-dimensional probabilistic wind-borne debris trajectory model for building envelope impact risk assessment. J. Wind Eng. Ind. Aerod. 102, 22–35.
Holmes, J.D., 2004. Trajectories of spheres in strong winds with application to wind-borne debris. J. Wind Eng. Ind. Aerod. 92, 9–22.
Holmes, J.D., Letchford, C.W., Lin, N., 2006. Investigations of plate-type windborne debris—Part II: computed trajectories. J. Wind Eng. Ind. Aerod. 94, 21–39.
ICC 500, 2014. Standard and Commentary: ICC/NSSA Design and Construction of Storm Shelters. International Code Council, Washington, DC.
Kakimpa, B., Hargreaves, D.M., Owen, J.S., 2012. An investigation of plate-type windborne debris flight using coupled CFD-RBD models. Part I: model development and validation. J. Wind Eng. Ind. Aerod. 111, 95–103.
Kakimpa, B., Hargreaves, D.M., Owen, J.S., Martinez-Vazquez, P., Baker, C.J., Sterling, M., Quinn, A.D., 2010. CFD modelling of free-flight and auto-rotation of plate type debris. Wind Struct. 13, 169–189.
Kordi, B., Kopp, G.A., 2011. Effects of initial conditions on the flight of windborne plate debris. J. Wind Eng. Ind. Aerod. 99, 601–614.
Kordi, B., Traczuk, G., Kopp, G.A., 2010. Effects of wind direction on the flight trajectories of roof sheathing panels under high winds. Wind Struct. 13, 145–167.
Kulkarni, A., Shafei, B., 2021. Ultra-high performance concrete building wall panels engineered to resist windborne debris impact. J. Build. Eng. 42, 1–14, 103004.
Lin, N., Holmes, J.D., Letchford, C.W., 2007. Trajectories of wind-borne debris in horizontal winds and applications to impact testing. J. Struct. Eng. 133, 274–282.
Minor, J.E., 1994. Windborne debris and the building envelope. J. Wind Eng. Ind. Aerod. 53, 207–227.
Murman, S., Aftosmis, M., Rogers, S., 2005. Characterization of space shuttle ascent debris using CFD methods. Proc. 43rd AIAA Aero. Sci. Meet. Exhib. 1–20.
Richards, P.J., Hoxey, R.P., 1993. Appropriate boundary conditions for computational wind engineering models using the k-ε turbulence model. J. Wind Eng. Ind. Aerod. 145–153, 46–47.
Richards, P.J., Williams, N., Laing, B., McCarty, M., Pond, M., 2008. Numerical calculation of the three-dimensional motion of wind-borne debris. J. Wind Eng. Ind. Aerod. 96, 2188–2202.
Saini, D., Shafei, B., 2021. High-fidelity prediction of flight trajectories of plate-type debris in boundary layer winds. J. Wind Eng. Ind. Aerod. 217, 1–14, 104727.
Saini, D., Shafei, B., 2020a. Damage assessment of wood frame shear walls subjected to lateral wind load and windborne debris impact. J. Wind Eng. Ind. Aerod. 198, 1–13, 104091.
Saini, D., Shafei, B., 2020b. Performance of structural insulated panels with metal skins subjected to windborne debris impact. J. Compos. B. Eng. 198, 1–12, 108163.
Tachikawa, M., 1988. A method for estimating the distribution range of trajectories of wind-borne missiles. J. Wind Eng. Ind. Aerod. 29, 175–184.
Tachikawa, M., 1983. Trajectories of flat plates in uniform flow with application to wind-generated missiles. J. Wind Eng. Ind. Aerod. 14, 443–453.
Uchibori, K., Tamura, T., 2019. LES study on aerodynamics of auto-rotating square flat plate by IBM and SAMR. J. Fluid Struct. 89, 108–122.
Visscher, B.T., Kopp, G.A., 2007. Trajectories of roof sheathing panels under high winds. J. Wind Eng. Ind. Aerod. 95, 697–713.
Wills, J.A.B., Lee, B.E., Wyatt, T.A., 2002. A model of wind-borne debris damage. J. Wind Eng. Ind. Aerod. 90, 555–565.